Composites Science and Technology 256 (2024) 110782

Contents lists available at ScienceDirect

Composites Science and Technology

journal homepage: www.elsevier.com/locate/compscitech

Coaxial direct ink writing of ZnO functionalized continuous carbon fiber-reinforced thermosetting composites

Zhuoyuan Yang [a], Evan Medora [a], Zefu Ren [a], Meng Cheng [b,*], Sirish Namilae [a,**], Yizhou Jiang [a,***]

[a] Department of Aerospace Engineering, Embry-Riddle Aeronautical University, Daytona Beach, FL, 32114, USA
[b] Key Laboratory of Metallurgical Equipment and Control Technology, Ministry of Education, Wuhan University of Science and Technology, Wuhan, Hubei, 430081, China

ARTICLE INFO

Keywords:
Continuous carbon fiber
Coaxial direct writing
Additive manufacturing
Thermosetting composite
Interfacial strength

ABSTRACT

Additive manufacturing of fiber-reinforced thermosetting composites is of great importance for various applications. However, improving the quality of the fiber/matrix interface under various additive manufacturing processes is still in the early stages. Herein, for the first time, we report the coaxial direct ink writing of zinc oxide (ZnO) functionalized continuous carbon fiber-reinforced thermosetting polymer composites. Both elastomeric and rigid thermosetting polymers reinforced with ZnO functionalized continuous carbon fiber composites can be printed into single filaments with turning angles and multi-layer tall arbitrary structures. The printed ZnO functionalized epoxy composites achieve Young's modulus of 3.69 GPa, which is 15.3% higher than pristine fiber-reinforced composites. The printed composite exhibits resistance under various environmental conditions. Additionally, ZnO functionalization significantly enhances the fiber/matrix interface strength, with improvements of 57%. The reduced modulus of ZnO functionalized fibers is 174% higher than that of pristine fibers. ZnO nanowires enhance the heating transfer rate of carbon fibers by 17% within the same heating time. Our innovative coaxial direct ink writing offers a general strategy for multi-material printing, laying the groundwork for future additive manufacturing of functional composite devices and structures with enhanced performance.

1. Introduction

Fiber-reinforced polymer composites have been abundantly used in defense, aerospace, and energy storage devices in recent decades due to their excellent thermal stability, unparalleled mechanical strength, and robust chemical resistance [1–4]. To date, traditional production methods such as injection molding, filament winding, and pultrusion depend on costly molding tools to shape resin and fibers into desired forms [5–8]. These methods necessitate large-scale production to offset the expenses associated with assembly and labor, leading to the creation of complex designs or new materials considerably challenging.

Recent advances in 3D printing distinguish itself by enabling new fabrication methods of composite components [9–12], wherein the design complexity does not translate into higher costs. Various innovative additive manufacturing (AM) strategies have been developed to advance the fabrication of fiber-reinforced polymer composites [13–16]. These composites are classified based on the fiber aspect ratio [17] into short fiber and continuous fiber-reinforced types. Although the fabrication of composites reinforced with short fibers has been widely enabled via AM techniques, their application is limited due to the inferior mechanical performance, in contrast to composites reinforced with continuous fibers [15]. As a result, there is an increasing focus on the development of continuous fiber-reinforced polymer composite 3D printing.

As a reinforcement material, continuous carbon fibers possess highly desirable characteristics including high mechanical strength, low density, outstanding thermal conductivity, and electrical conductivity [18,19]. In terms of the polymer matrix, most studies focused on thermoplastic polymers and UV-curable thermosetting polymers due to the ease of manufacturing. For example, Thakur et al. [20] demonstrated a UV-assisted coextrusion deposition method for 3D printing continuous carbon fiber-reinforced photosensitive polymer composites, providing

* Corresponding author.
** Corresponding author.
*** Corresponding author.
E-mail addresses: chengmeng@wust.edu.cn (M. Cheng), namilaes@erau.edu (S. Namilae), yizhou.jiang@erau.edu (Y. Jiang).

https://doi.org/10.1016/j.compscitech.2024.110782
Received 16 March 2024; Received in revised form 20 June 2024; Accepted 30 July 2024
Available online 31 July 2024

the possibility to improve the mechanical properties of battery structures. Heidari-Rarani et al. [21] analyzed the mechanical properties of continuous carbon fiber-reinforced polylactic printed by a commercial fused deposition modeling using a modified nozzle. As reliable matrix materials in composites with high-temperature resistance and superior mechanical performance [22], pure thermosetting polymers, like pure epoxy and silicone rubber, have higher fabrication complexity due to the slow and irreversible solidification process. Direct ink writing (DIW) methods have been introduced to print pure thermosetting material [23]. As an extrusion-based AM method, DIW stands out for printing liquid-state materials [24]. For instance, He et al. [25] introduced an innovative extrusion design for a DIW 3D printer and analyzed the shear forces exerted on the fibers by modifying the rheological properties of the ink and controlling the secondary pressure.

Tuning the rheological properties of composite matrices in DIW is a proven method to achieve 3D printing of continuous fiber-reinforced thermosetting composites. However, to our best knowledge (Table S1), few studies have focused on functionalizing carbon fibers to improve the fiber/thermosetting matrix interface quality under various AM process controls [26 28]. Functionalized fibers can also enhance the mechanical properties and structural integrity of the printed thermosetting composite materials, mitigating issues like delamination or reduced mechanical strength to a certain extent. It is not surprising that there have been many methods to alter the surface of carbon fibers [29] within a composite to improve the interface with the matrix. One of the more successful methods is to grow zinc oxide (ZnO) nanowires on the surface of the fibers [30 32]. The objective of cultivating fur-like rod--shaped ZnO nanowires around the carbon fibers is to significantly increase the effective surface area of the coated fibers, which then forms strong bonds among the fibers, ZnO nanowires, and polymer [30].

Additionally, there are many variations of the process for growing the ZnO nanowires. In general, the ZnO nanowires can be grown in a relatively low-temperature aqueous solution without thermal degradation [31]. In terms of strength enhancement, recent studies regarding the chemical processes have shown significant improvements in interfacial shear strength [8,30,33]. It was also shown that growing ZnO nanowires on chemically treated carbon fiber prepreg sheets improved thermal conductivity, which could be a significant advantage in the context of continuous fiber printing using thermosetting polymers [34, 35].

In this report, we have engineered a coaxial DIW 3D printer by modifying a robotic dispensing system to facilitate the printing of thermosetting polymer composites, which are notably reinforced with ZnO-functionalized continuous carbon fibers. The rheological properties of the printable thermosetting polymer composite inks were well-tuned to precisely control the morphology of the extruded filaments. Multiple test cases, including single filaments with turning angles and multi-layer tall arbitrary structures, have conclusively demonstrated the exceptional printing capabilities of the proposed coaxial DIW process using both elastomeric and rigid thermosetting polymers. The printed rigid samples achieved Young s modulus of 3.69 GPa, demonstrating consistent mechanical properties after exposure to various environmental conditions. The bonding strength remained well-maintained after different mechanical deformations, confirming the stability of the composites fabricated by our coaxial DIW method. Nanoindentation tests indicated that ZnO nanowires on the fibers improve the interface strength between fibers and matrix by up to 57%. Accelerated Property Mapping (XPM) revealed that ZnO functionalized fibers exhibited a reduced modulus of 49.99 GPa, which is 174% higher than untreated fibers. Furthermore, incorporating ZnO nanowires into continuous carbon fibers improved their thermal conductivity, increasing the heating rate of carbon fibers by 17% within the same duration, thus enhancing the in-situ curing efficiency of thermosetting polymers. These findings expand the potential of continuous fiber additive manufacturing, paving the way for the development of functional devices with significantly enhanced interfacial properties through multi-material printing techniques.

2. Experimental

2.1. Coaxial DIW setup and printing process control

To realize the proposed 3D printing process for ZnO functionalized continuous carbon fiber thermosetting composites, we customized a coaxial extrusion nozzle, which was mounted on a motorized XYZ three-axis dispensing robot (5552202-Dispensing Robot, Integrated Dispensing Solutions, USA), as shown in Fig. 1a. The coaxial extrusion system consists of a fiber feeder to guide the prepreg continuous carbon fibers, flanked by two pneumatic ink dispensing syringes for thermosetting extrusion. Impregnation is accomplished by submerging ZnO functionalized fibers into a thickener-free matrix material (Fig. S1), followed by centrifuging at 5000 rpm for 3 mins. The prepreg fibers are then carefully wrapped onto the fiber feeder using tweezers. The design of the fiber feeder guarantees an adequate length of printable fibers. The air pressure for ink dispensing syringes is adjustable from 0 to 100 psi. The dispensing process was implemented by extruding inks through coaxial nozzle tips onto a moving substrate in a filament-by-filament and layer-by-layer way. It can precisely control the deposition speed v, and the standoff distance h, between the printing nozzle and the substrate (Fig. 1b).

The coaxial nozzle was designed using 3D computer-aided design software (SolidWorks). The model was printed using a stereolithography 3D printer (Saturn 2 8K, ELEGOO, USA). All nozzles were printed with ELEGOO standard translucent resin with a layer thickness of 50 m. After printing, the coaxial nozzles were rinsed with 99% isopropyl alcohol using a long-handled washing bottle to clean the channels. The coaxial nozzles were then dried in a vacuum oven at 50 C for 8 h. The inner outlet for fiber feeding has a diameter of 0.5 mm. The outer outlet for ink extrusion is 3 mm in diameter, with a separating wall of 0.1 mm thickness at the coaxial nozzle tip, which is the minimum reliable printing dimension for a stereolithography 3D printer (Fig. S2). Additionally, a silicon heater film is integrated into the printing platform of the robot, allowing temperature adjustments ranging from 25 to 150 C. The in-depth schematic views of the internal structure of the filament are shown in Fig. 1c. The Outer matrix layer is the composite matrix, and the Inner layer uses the same base material without a thickener for prepreg purposes. It illustrates the schematic cross-section of the extruded filament and ZnO functionalized carbon fibers fully embedded in the matrix material.

All print paths were initially designed in SolidWorks to precisely determine the XY coordinates. Aligned with the specified coordinates, the G-Code required to control the motion of the nozzle was programmed via the external teach pendant.

2.2. Preparation of ZnO functionalized fiber

ZnO functionalized carbon fibers were achieved through a hydrothermal process, building on the foundation of our previous work [36], demonstrating stability and consistency. Several other research groups have also reported on the reliability and repeatability of this process [30, 37 41]. ZnO nanowire growth on carbon fibers involves four stages (Fig. 2a): desizing, acid activation, seeding, and growing. The related morphologies of fiber are illustrated in Fig. 2b. SEM images of the resulting ZnO nanowires grown on a single carbon fiber are shown in Fig. 2c. Notably, by controlling the pre-immersion time of the fibers, we can achieve fibers functionalized with varying degrees of ZnO, categorized as pristine fibers, partially functionalized fibers, and fully functionalized fibers. The detailed procedure steps are provided in the Supplementary Information.

2.3. SEM imaging of ZnO functionalized fiber

The levels of the ZnO functionalized fiber were inspected utilizing Scanning Electron Microscopy (SEM) (FEI Quanta 650, USA). A thin

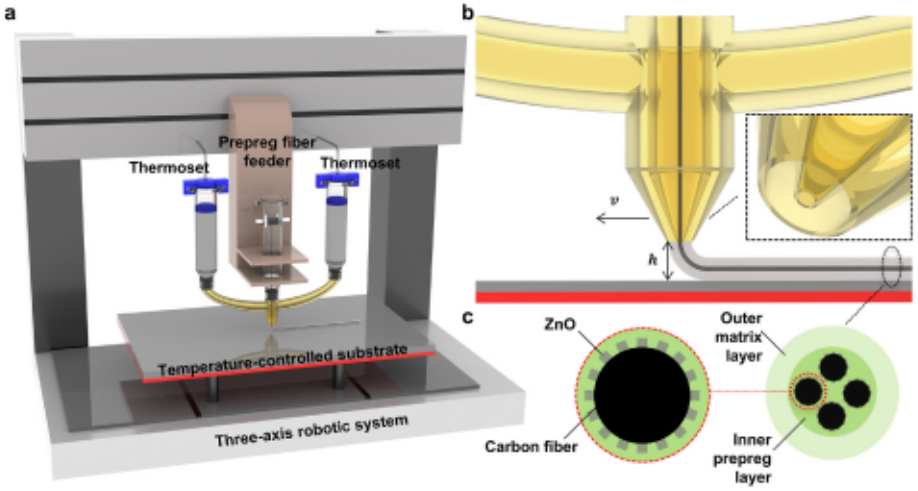

Fig. 1. Overview of coaxial direct ink writing of ZnO functionalized continuous carbon fibers. (a) Schematic illustration of a coaxial direct ink writing system. (b) Coaxial nozzle design. (c) Cross-section of ZnO functionalized carbon fibers embedded in the matrix.

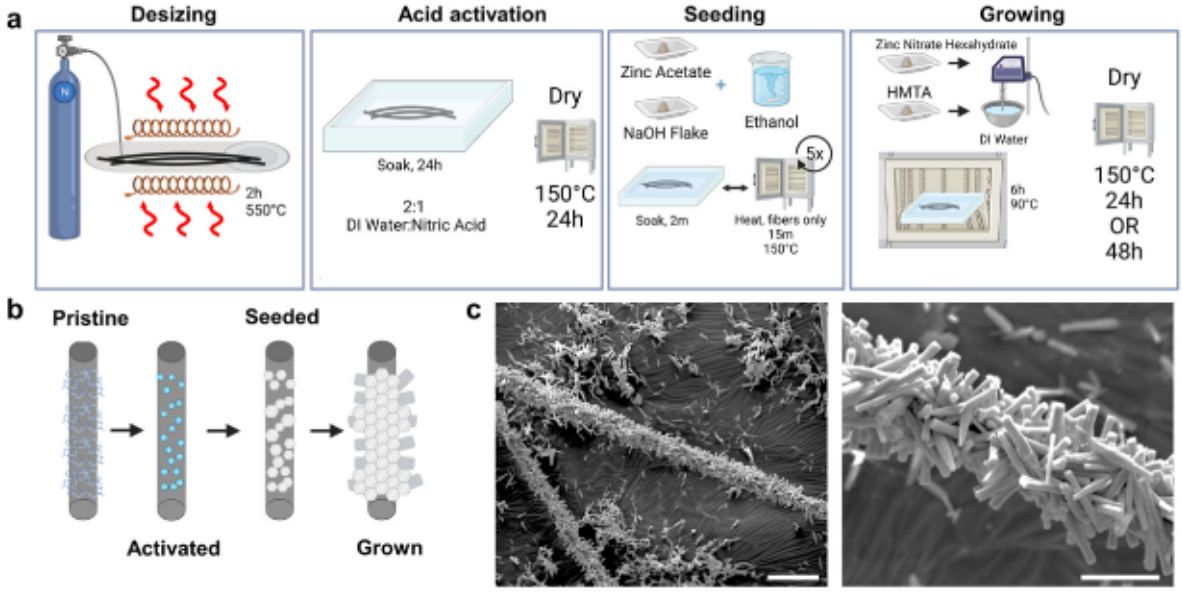

Fig. 2. The stepwise fabrication of ZnO functionalized continuous carbon fiber. (a) Preparation workflow. (b) Schematic illustration of ZnO nanowire cultivation. (c) SEM of ZnO functionalized carbon fiber at length scales. Scale bar: 10 μm.

layer of gold (10 nm) was uniformly coated onto the samples using a Manual Sputter Coater (Ted Pella, Redding, USA). All SEM images were captured at an acceleration voltage of 20 kV and a working distance of around 10 mm.

2.4. Preparation of thermosetting polymer ink

Both elastomeric and rigid thermosetting polymer inks were prepared. For the elastomeric thermoset, we selected Dragonskin 30 ink (Smooth-on, USA) with the addition of the rheology modifier THI-VEX (Smooth-on, USA) for printing demonstrations. For the rigid thermoset, we selected epoxy (Aeropoxy PR3665, USA) ink with fumed silica nanoparticles incorporated as rheology modifiers for printing demonstrations; BioPoxy36 (EcoPoxy, USA) was used for interfacial behavior characterization. Further details on rheological characterization and differential scanning calorimetry (DSC) test of these thermosetting inks are provided in the Supplementary Information.

2.5. Mechanical properties for epoxy and elastomer composite

The epoxy composites used for tensile tests were printed by our coaxial direct writing technique. Different degrees of ZnO coating on carbon fiber-reinforced epoxy composites were achieved using carbon fibers with corresponding coating levels defined as printed-pristine, printed-partially, and printed-fully. Treated epoxy filaments were subjected to various environmental conditions on printed-fully samples: placed in an oven at 120 °C for 24 h, in a freezer at −20 °C for 24 h, in a humidity-controlled chamber at 90% relative humidity (RH) for 24 h, and in a humidity-controlled chamber at 15% RH for 24 h. After treatment, all samples were subjected to room temperature (23 °C and 50% RH) and equilibrated for at least 2 h. The samples were defined as follows: 120 °C treated, −20 °C treated, 90% RH treated, and 15% RH treated.

The elastomer composites were used for bonding force tests. Molded samples were fabricated by the injection molding method, while printed samples were produced using our coaxial direct writing technique. Samples reinforced by different degrees of ZnO coating carbon fibers

were created into categories as molded-partial, molded-fully, printed-partial, and printed-fully. Printed-fully samples subjected to 1000 cycles of ±90° bending or 20 turns/m longitudinal twisting were defined as after-bend and after-twist, respectively. The detailed sample preparation and test procedures are provided in the Supplementary Information.

2.6. Fiber/matrix interfacial behavior characterisation

The impact of ZnO functionalization on interface strength was characterized through nanoindentation and XPM via the nanomechanical test system (Fig. S3a) (Hysitron TI 980 TriboIndenter, Bruker, Germany). Additional details on the nanoindentation samples preparation (Fig. S3b), characterization procedures (Fig. S4), and complete calculation are reported in the Supplementary Information.

3. Results and discussion

3.1. Thermal behavior of ZnO functionalized fiber

To investigate the role of ZnO functionalized continuous carbon fibers in the printing process, we compared the thermal behaviors of three types of fibers, with varying degrees of ZnO nanowire functionalization. The experimental setup depicted in Fig. S5a is designed to explore the impact of ZnO nanowire functionalization on the thermal conductivity of 1k fiber tow. The SEM images of ZnO nanowires gradient on fiber surfaces are depicted in Fig. 3a. In SEM images, two distinct patterns in the microstructure were observed: the ZnO nanowires almost invariably adopt a spike-like formation upon attachment to the carbon fibers, anchoring at one end and extending outward at a steep angle. Furthermore, clusters of ZnO nanowires frequently emanate from a single site. These clusters are some of the initial formations growing from the "seeds" created during the seeding process. When the fibers are fully coated the seeded nanowires can grow enough to interconnect and cover most of the surface area of the fiber. Partially functionalized fibers have fewer nanowires overall.

This phenomenon is depicted alongside their thermal profiles observed after heating for 3 s, as shown in Fig. 3b, demonstrating the thermal characteristics of the fibers in response to the nanowire growth and coverage. The thermal distribution profiles show marked differences in heat transfer among fibers with different degrees of coating. Specifically, pristine fibers exhibited the lowest thermal transfer efficiency, reaching 62.6 °C after heating for 3 s at an equilibrium temperature of 85 °C. Within the same time frame, partially functionalized fibers exhibited average thermal conductivity, attaining 68.3 °C. Fully functionalized fibers demonstrated the highest thermal conductivity, reaching 69.6 °C.

All three types of fibers exhibit a similar heating trend characterized by a rapid quick increase initially followed by a slower rise towards the end. However, within the same timeframe, fibers functionalized with ZnO nanowires reach temperatures 5–10 °C higher (up to 17% faster) than those of pristine fibers (Fig. 3c). This improvement is attributed to the growth of ZnO nanowires on the fibers, which serve as nanoscale heat bridges between them (Fig. S5b) facilitating improved thermal transfer abilities [35]. We also found that fibers with partial ZnO nanowire coatings, within the same 5 s period, have slightly lower heat transfer efficiency, typically 2–3 °C lower than fully functionalized fibers. This observation further supports the role of ZnO nanowires in enhancing thermal transfer among fibers. Consequently, this enhanced thermal transfer capability aids in reducing the curing time of extruded thermosetting composite filaments. Therefore, ZnO functionalization is crucial for optimizing the manufacturing workflow of the proposed method.

3.2. Rheological and curing properties of thermosetting polymer inks

In this part, we tested both elastomeric and rigid thermosetting polymer inks for our coaxial DIW method. First, we formulated an elastomeric thermosetting ink using Dragonskin 30 silicone rubber with 2 wt.% thickener added, which serves as a rheological modifier. Upon increasing the shear rate from 0.1 s^{-1} to 100 s^{-1}, the apparent viscosity of the unmodified silicone ink decreased from 16.4 Pa-s to 8.8 Pa-s. In contrast, the apparent viscosity of the rheologically modified silicone ink showed a more dramatic reduction from 2253.3 Pa-s to 18.3 Pa-s (Fig. 4a). The modification substantially improved the shear-thinning behavior compared to the unmodified silicone ink, to ensure high geometrical stability at low shear rate to maintain fiber alignment at the center of the nozzle.

Further, a comparative analysis of the storage and loss modulus between silicone with and without thickener is depicted in Fig. 4b. Notably, the unmodified silicone lacks viscoelastic properties [42,43], as indicated by the absence of an intersection of storage modulus and loss modulus ($G' = G''$) in the entire oscillation stress range. Conversely, the modified silicone ink displays solid-like properties. At low oscillation stress range (<200 Pa), storage modules ($G' = 60.7$ kPa) are much larger than loss modulus ($G'' = 10.1$ kPa). When the oscillation stress exceeds 200 Pa, the storage modulus becomes less than the loss modulus, and the ink begins to flow. This suggests that the modified silicone ink can easily be extruded by pneumatic pressure through the nozzle and rapidly retain a stable filamentous shape upon returning to no-shearing conditions.

Beyond rheological properties, rapid curing is also crucial for the precision of 3D-printed continuous carbon fiber composites. The curing performance of silicone ink was tested under varied heating rates of 5, 25, and 45 °C/min using DSC machine, respectively. The sigmoidal curve in Fig. 4c is representative of an autocatalytic reaction mechanism. This curve distinctly illustrates a significant increase in the curing rate as the heating rates rise, which gives us a guideline for 3D printing

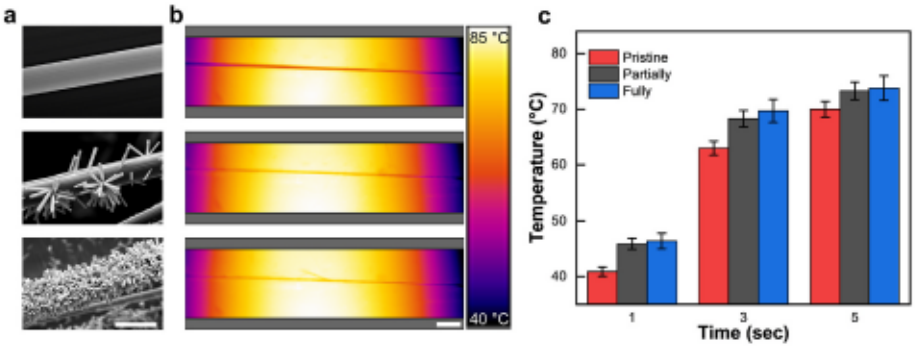

Fig. 3. Thermal behaviors of ZnO functionalized fiber. (a) Surface morphologies of pristine, partially functionalized, and fully functionalized carbon fiber. Scale bar: 10 μm. (b) Thermal profiles after heating for 3 s. Scale bar: 10 mm. (c) Bar graph for quantifying the thermal profiles.

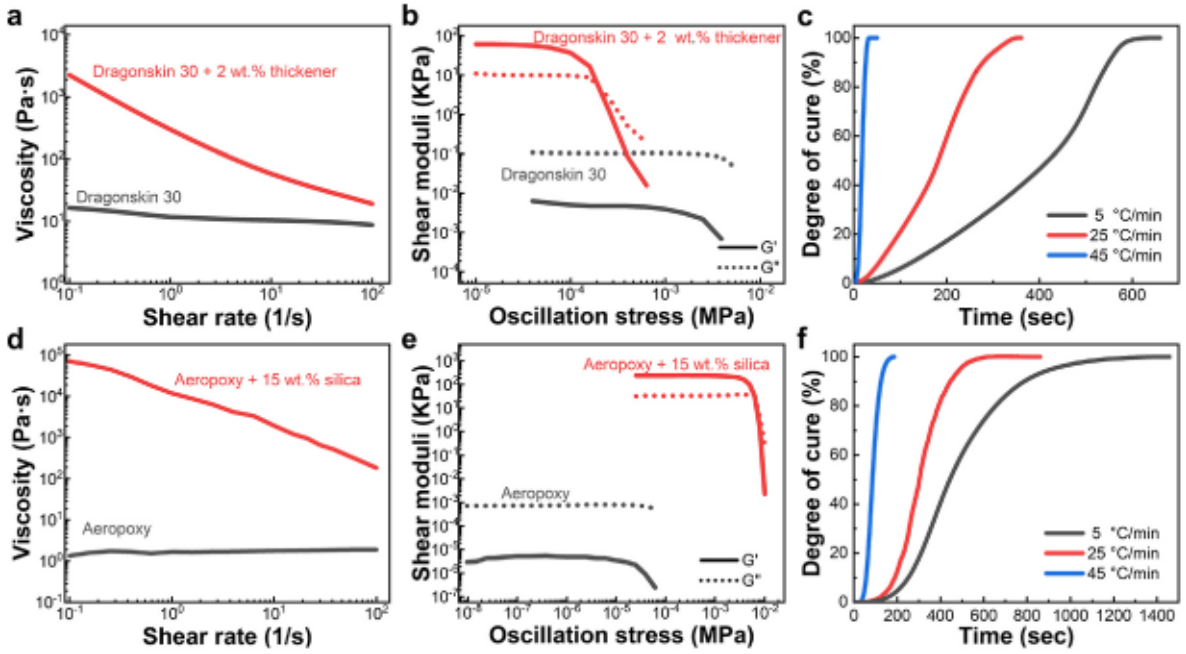

Fig. 4. Rheological and curing properties analysis. (a) Log-log plot of apparent viscosity as a function of shear rate for Dragonskin 30 silicone ink with and without 2 wt.% thickener modification. (b) Storage moduli G′ and loss moduli G″ as a function of shear stress for Dragonskin 30 silicone ink with and without 2 wt.% thickener modification. (c) Degree of cure as a function of time for the Dragonskin 30 silicone ink. (d) Log-log plot of apparent viscosity as a function of shear rate for Aeropoxy resin ink with and without 15 wt.% silica. (e) Storage moduli G′ and loss moduli G″ as a function of shear stress for Aeropoxy resin ink with and without 15 wt.% silica. (f) Degree of cure as a function of time for the Aeropoxy resin ink.

applications, particularly when fast curing is needed for maintaining print integrity.

Similarly, we performed the same characterization on rigid thermosetting polymer inks. In this study, we selected Aeropoxy and 15 wt.% fumed silica nanoparticles as a rheological modifier. By incorporating silica nanoparticles, the ink with initial near-Newtonian behavior [42] acquired shear-thinning properties, as illustrated in Fig. 4d. When the shear rate increased from 0.1 s^{-1} to 100 s^{-1}, the apparent viscosity of the modified epoxy ink dropped from 70782.4 Pa·s to 183.5 Pa·s. At low shear forces, this significant apparent viscosity ensures that the extruded filaments do not flow during the initial deposition stage. As shown in Fig. 4e, unmodified Aeropoxy ink exhibits liquid-like behavior.

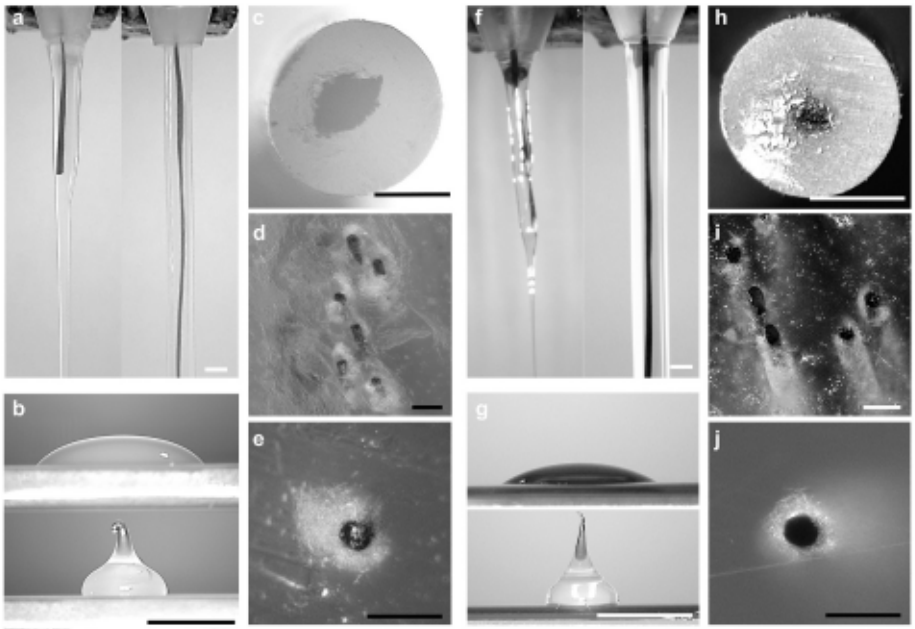

Fig. 5. Morphology of thermosetting polymer inks through extrusion. (a) Filament extrusion behavior of unmodified and modified silicone inks. (b) Single-droplet deposition test of the silicone inks. (c) Large-scale filament cross-section view of modified silicone ink. (d, e) High-magnification cross-section view of ZnO-functionalized carbon fibers embedded in a silicone matrix. (f) Filament extrusion behavior of unmodified and modified epoxy inks. (g) Single-droplet deposition test of the epoxy inks. (h) Large-scale filament cross-section view of modified epoxy ink. (i, j) High-magnification cross-section view of ZnO-functionalized carbon fibers embedded in an epoxy matrix. Scale bar: (a–c) 1 mm. (d, e) 20 μm. (f–h) 1 mm. (i, j) 20 μm.

However, Aeropoxy ink with 15 wt.% silica nanoparticles content transitions to solid-like properties, with a shear yield stress and storage modulus of 5.311 kPa and 239 kPa, respectively. The rheological results also confirm that modified Aeropoxy is suitable for coaxial continuous carbon fiber 3D printing. In addition, we assessed the curing rate of Aeropoxy resin ink under identical thermal conditions using DSC machine (Fig. 4f). The curing rate of the Aeropoxy resin ink is slightly slower than that of silicone ink, but still can be solidified within minutes.

Notably, rheological and curing testing not only characterizes the inherent properties of the material but also provides guidance for setting printing parameters. Although both are physically different solid-like liquids, by changing the printing parameter settings, our proposed DIW method has the full capability to print them.

3.3. Morphology of thermosetting polymer inks through extrusion

In this study, we also investigated the influence of matrix rheological properties for both elastomeric and rigid thermosetting polymers on the geometrical morphologies of the filaments during our DIW process. We first studied the morphology of filaments extruded from two types of silicone formulation inks, using identical extrusion pressure (15 psi), as illustrated in Fig. 5a. The modified silicone ink, in contrast to the unmodified silicone, exhibited a remarkable capacity to maintain the filament in a cylindrical shape. This observation indicates that modified silicone has shear yield stress, which is consistent with previously mentioned rheological results. We also found that the presence of the shear yield stress helps prevent the ink from dripping through the coaxial nozzle before and during printing.

To evaluate the influence of rheological properties modifications on silicone deposition during printing, a single droplet was extruded through a 2 mm diameter stationary tapered nozzle by the dispensing robot onto glass plates coated by polyimide tape (Fig. 5b). After dropping a dot, the unmodified silicone spread out into a nearly flat shape, indicating the absence of viscoelastic properties. In contrast, the modified silicone formed and maintained a teardrop geometry, reflecting higher structural integrity and shape retention due to the shear yield stress. Such capability enables resistance to deformation under gravity and surface tension after depositing. Moreover, void-free fiber impregnation is crucial for efficient load transfer, which is essential for the fabrication of high-quality fiber-reinforced composites. The cross-section of the extruded tow is shown in Fig. 5c e, revealing that the silicone ink has fully penetrated the ZnO functionalized fiber tow. This demonstrates that our ink formulation and extrusion process successfully achieved the desired interfacial bonding between the matrix and fibers, which is critical for the mechanical integrity of the resulting composite.

Following the methodology applied to silicone ink studies, we examined the extrusion behavior of epoxy-based ink under similar conditions, increasing the extrusion pressure to 55 psi. As shown in Fig. 5f, the silica-modified epoxy resin ink demonstrated an excellent ability to maintain structural integrity post-extrusion, forming filaments with a consistent cylindrical shape, indicating that the epoxy matrix has achieved the optimized rheological properties. To determine the impact of rheological adjustments on the deposition of epoxy ink, we replicated the single-droplet deposition test with epoxy ink. Unlike the modified silicone, the modified epoxy ink maintained a more distinct cohesive form (Fig. 5g), aligning with the higher shear yield stress and enhanced viscoelasticity observed in rheological testing. This test further validated the successful modification of the rheological properties of the epoxy resin ink, making it suitable for precision 3D printing applications. By analyzing the cross-section of the extruded filaments to assess impregnation quality, the epoxy resin ink exhibited effective penetration into the fiber bundles (Fig. 5h j). This level of impregnation is akin to the void-free interfacial adhesion achieved with silicone inks. These findings validate the efficacy of our coaxial nozzle design in ensuring high-quality fiber impregnation.

These results confirm that by incorporating rheological modifiers, thermosetting materials, previously considered unsuited for coaxial continuous carbon fiber composite 3D printing, can be adapted to ink with shear-thinning and viscoelastic properties. Such modifications of thermosetting ink expand our ability to select and tailor a wide range of materials for diverse printing applications.

3.4. Printing process control, demonstrations, and mechanical properties

The filament extrusion is driven by the shear force applied by the ink on the fiber bundle. In the Supplementary Information (Figs. S6 S8), the shear force on the fiber bundle is calculated based on the measured filament extrusion speed. To evaluate the feasibility of the coaxial printing method, we initially focused on the realizability of printed corners, which are crucial in the DIW of continuous fiber composites. As the extruded filaments go through corners, the fiber bundle rotates inside the filamentary matrix material. This rotation induces internal stresses in the fibers, leading to deviations within the composite filament. Such misalignment significantly impacts both the print quality and the mechanical properties of the manufactured final parts [25,44]. This issue is further magnified owing to the shear-thinning characteristics of the matrix.

An optimized printing method was proposed for the thermosetting characteristics of thermosetting materials. This method effectively reduces the impact of internal stresses in the fibers, thereby enhancing the dimensional accuracy of corners. As discussed in Section 3.2, our thermosetting matrix can cure in just a few seconds. Generally, once the degree of cure exceeds 60%, thermosetting ink is considered to transition to a gel-like state. At this point, the viscosity of the resin increases from a finite value to infinity. Consequently, the internal stresses in the fibers are much lower than the shear yield stress of the ink in its gel-like state. Therefore, utilizing the rapid curing characteristics of the ink can address the issue of corner printing failures and offer the possibility of in-situ solidification.

In our test cases, all samples were fabricated in a continuous single path. Before printing, the material was pre-extruded for 2 s to ensure consistent flow. After printing, the fiber was cut with scissors. All test cases were printed on glass plates covered with high-temperature polyimide tape. Considering the diverse rheological properties of the extruded inks, we tailored the printing parameters according to the specific characteristics of each ink. For elastomer-based continuous carbon fiber printing, the printing speed was set to 15 mm/s. The deposition pressure was adjusted to 25 psi. The temperature of the substrate remained at 135 C. The layer thickness was established at 2 mm. For epoxy resin-based continuous carbon fiber printing, the printing speed was calibrated to 3 mm/s. Deposition air pressure was set to 50 psi. The temperature of the substrate remained at 135 C. The layer thickness was established at 1.5 mm.

As illustrated in Fig. 6a, silicone ink was utilized for the demonstration. Corners were successfully printed at four different angles: 180 , 135 , 90 , and 45 . This uniformity of filaments and consistent fiber alignment, as evident in the printed angles, further demonstrates the precision and reproducibility of our optimized printing method.

To further validate our capability in thermosetting composite materials 3D printing with ZnO functionalized continuous carbon fibers, both three-layered squares and circles were fabricated using both epoxy and silicone inks, as shown in Fig. 6b and c. The square samples had a side length of 50 mm, and the circular samples had a diameter of 50 mm. For the silicone samples, each layer was established at 2 mm in height; for the epoxy samples, each layer was established at 1.5 mm in height. The cross-section of the three-layered samples, as shown in Fig. 6d, reveals that the fiber was precisely centered within each filament, with consistent layer heights in both silicone and epoxy ink. As shown in our printing process control studies (Figs. S9 and S10), fine-tuned control over filament width was achieved by adjusting nozzle speed and pneumatic pressure, demonstrating the capability to locally customize

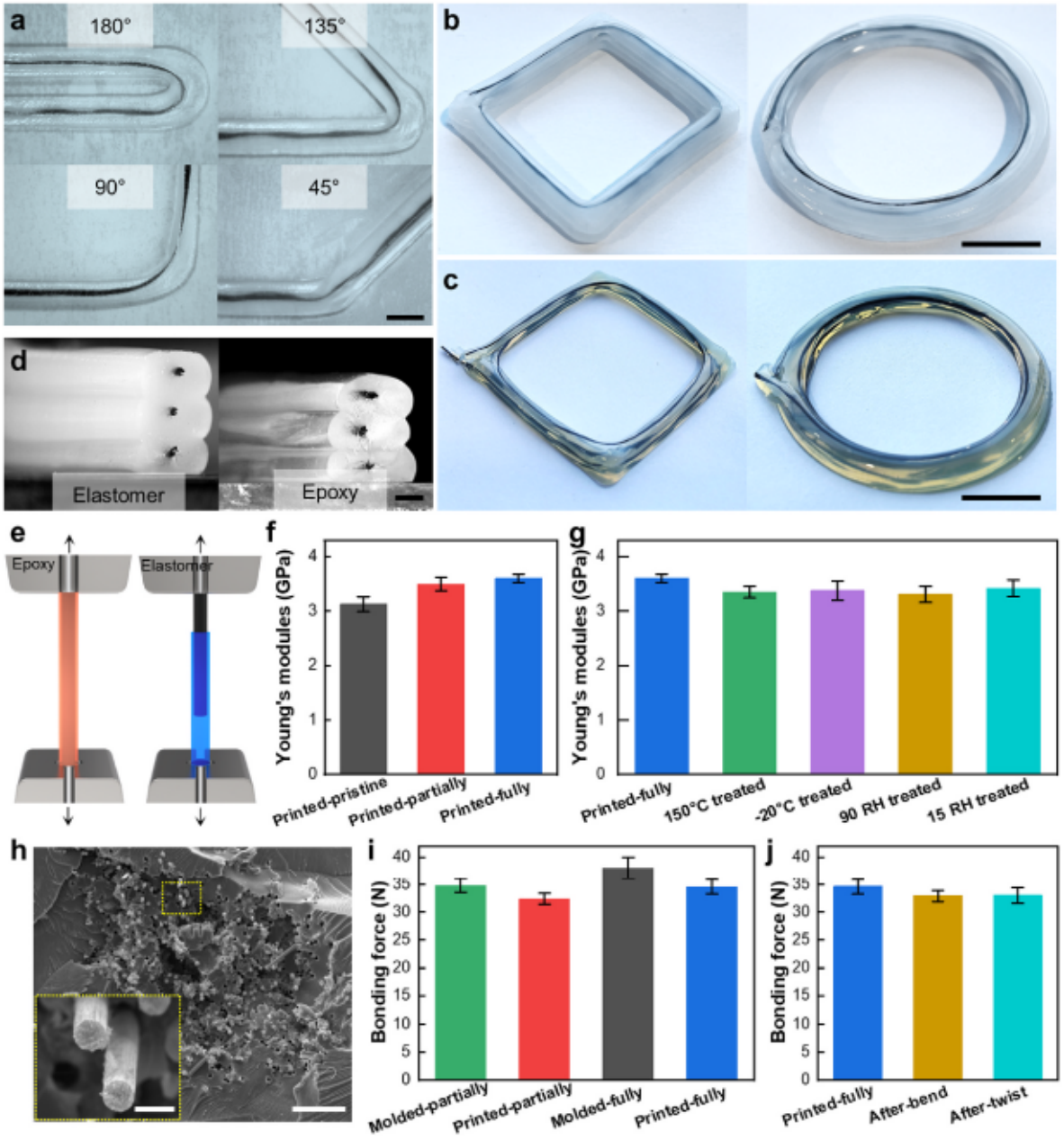

Fig. 6. Printing process control, demonstration, and mechanical properties. (a) Printed silicone composite at four distinct angles (180°, 135°, 90°, and 45°). Scale bars: 5 mm. (b, c) Three-layered geometric shapes (squares and circles) using modified silicone and epoxy inks. Scale bars: 10 mm. (d) Cross-sectional view of the layered structures in both silicone and epoxy samples. (e) Schematic of rigid epoxy filament tensile and elastomeric filament bonding force testing setup testing setups. (f) Young's modulus of printed filaments reinforced by pristine, partially functionalized, and fully functionalized carbon fiber. (g) Young's modulus of printed epoxy filaments under different treatments. (h) Tensile fracture surface of functionalized carbon fiber-epoxy filament. (i) Bonding force of elastomeric composite filaments fabricated using different methods. (j) Bonding force of printed elastomeric filaments under different deformation conditions. Scale bars: (a–d) 1 mm. (h) 100 μm, inset: 10 μm.

material properties.

To show the improved interfacial bonding enhanced by ZnO nanowires, the mechanical strength of the printed rigid epoxy filaments, reinforced with the different degrees of ZnO nanowires coated fibers, were compared (Fig. 6e). The filaments reinforced with fully functionalized carbon fiber exhibited Young's modulus of up to 3.69 GPa, representing an average increase of 15.3% compared to those reinforced with pristine fibers (Fig. 6f and Fig. S11). This enhancement in mechanical properties is attributed to the stronger interfacial strength provided by ZnO functionalization and aligns well with previous studies [45–48]. The mechanical properties of extruded ZnO-functionalized continuous carbon fiber-reinforced epoxy composites were thoroughly characterized to assess their response to different environmental conditions. Samples treated for 24 h at 150 °C, −20 °C, 90% RH, and 15% RH showed slight variations, with nominal values of 3.35 GPa, 3.37 GPa, 3.30 GPa, and 3.41 GPa, respectively (Fig. 6g and Fig. S12). Notably, the reductions in modulus were all within 10%, indicating that the printed epoxy filaments possess excellent environmental resistance. Only a few residual ZnO nanowires are observed at the tensile fracture interface (Fig. 6h), suggesting that the polymer matrix infiltrated the ZnO functionalized interface region, and the ZnO nanowires were embedded in the polymer matrix during fracture. The higher interface strength and increased stiffness contributed to the enhanced mechanical properties.

To demonstrate the reliability and robustness of our coaxial direct

writing technique in manufacturing composites, we tested the bonding force (Fig. 6e, Figs. S13–S15) between silicone and fiber produced by injection-molded and our DIW methods. The bonding force of printed-fully was 35 N, which is comparable to the bonding force of molded-fully (Fig. 6i and Fig. S13). Similar results were observed in partially functionalized samples. Additionally, the bonding force of the printed samples was tested after different mechanical deformations, specifically 1000 cycles of bending and 1000 cycles of twisting. The results show that the bonding force was well maintained within the margin of error (Fig. 6j and Fig. S14). Even after continuous bending and twisting for 1000 cycles, the samples maintained their bonding strength and could still lift a 1 kg weight (Fig. S15c).

In summary, this precisely controllable fabrication process has been successfully applied to a diverse range of thermosetting materials (from silicone to epoxy ink). Our DIW printing method not only conclusively demonstrates the adaptability and precision, but also underscores its potential in advancing the field of thermosetting composite material manufacturing, paving the way for innovative applications across various industries.

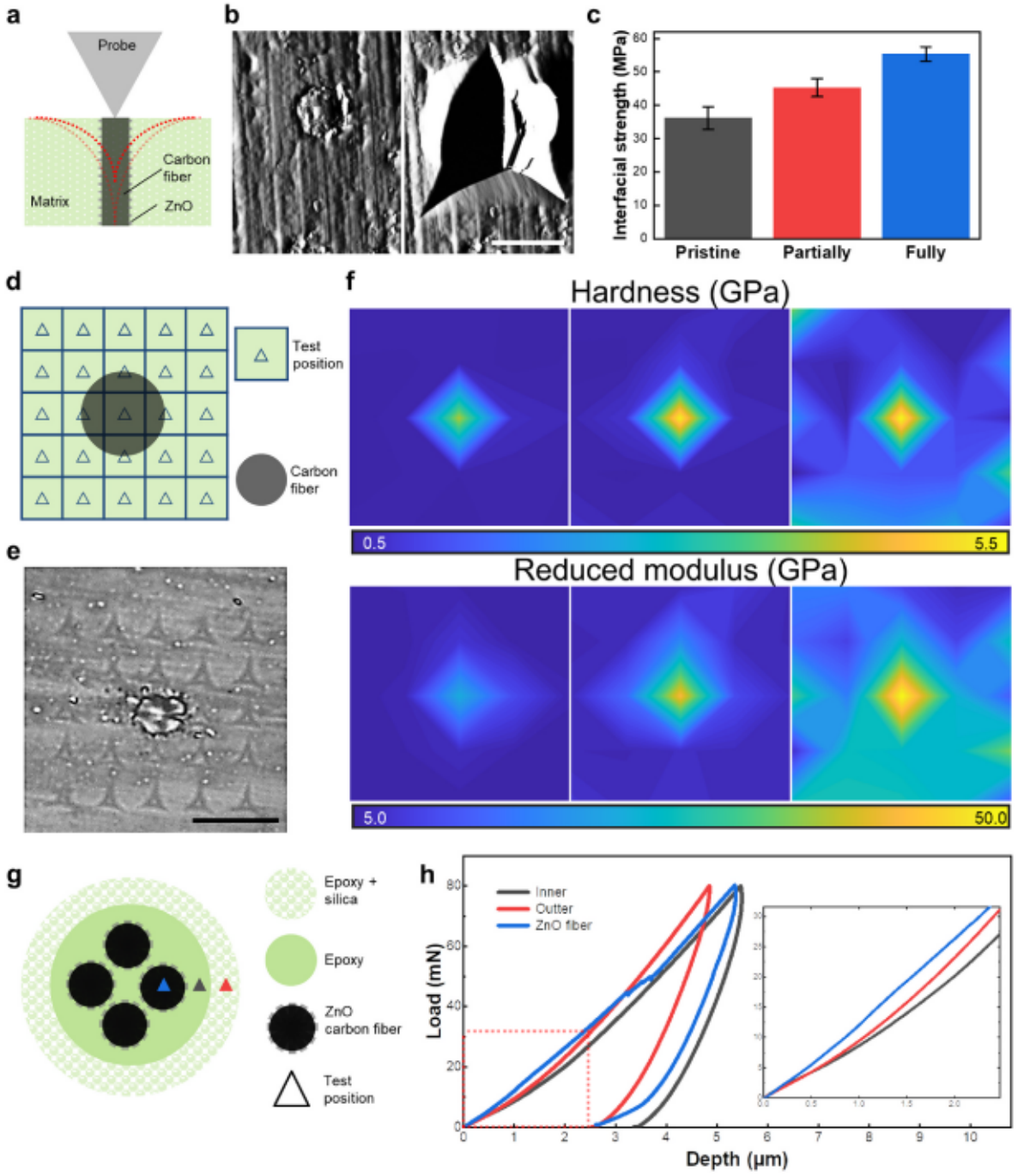

Fig. 7. Interfacial behavior of fiber/matrix. (a) Schematic of nanoindentation test on carbon fiber. (b) Before and after scans of the fiber and indentation area tested by the probe of the nanoindenter. Scale bar: 10 μm. (c) Interfacial strength for different fiber treatments. (d) Schematic of indentation positions for the XPM tests. (e) Optical images of fiber and surrounding epoxy after an XPM test. Scale bar: 10 μm. (f) XPM Hardness and reduced modulus results for (left to right) pristine, partially functionalized, and fully functionalized fibers. (g) Schematic of carbon fiber cross-section and surrounding epoxy when written with the coaxial nozzle which shows the silica-rich outer region. (h) Load-depth curves for the three distinct regions of the composite created by the coaxial nozzle.

3.5. Interfacial behavior of ZnO functionalized fiber

Different techniques are utilized for analyzing interface mechanics of fiber-matrix interfaces [49 51]. As shown in Fig. 7a, push-out tests were performed by pushing the fiber through the polymer matrix until debonding occurs via nanoindentation. The shear strength was determined by analyzing the load applied to the fiber tip and the depth of indentation [52]. The use of this micro-characterization system enables precise localized measurement, as well as facilitating direct characterization through optical and scanning based characterization methods. Additionally, because of the versatility of this approach, it has been used in many investigations with different material systems [53 60]. In our study, a force of 80 mN was applied to push the fibers into the matrix surface. Nonlinearities in the load-displacement curve indicating the fiber-matrix separation were observed well below the maximum load [54]. The force response during this action is recorded, and the debonding load for the fiber is determined. A comparison of a single fiber before and after indentation is displayed in Fig. 7b. In this study, we tested the pristine, partially functionalized, and fully functionalized carbon fibers (Fig. 7c). As a result, the fully functionalized fiber has the highest debonding load at an average of 72.85 mN. Compared to the pristine fiber, the calculated interfacial strength of the fully functionalized fiber increased by 57%. Such enhancement is attributed to the mechanical interlocking provided by ZnO nanowires.

To compare the hardness and reduced moduli between pristine and ZnO functionalized fibers, XPM was utilized. The testing area of XPM was set to focus on the central fiber and the surrounding epoxy surface. A square grid of 25 indents was used to plot out a 25 25 m^2 area around each type of fiber (Fig. 7d e). Through the comparison of XPM analysis results (Fig. 7f), we found that ZnO functionalization increased the hardness of the fibers from 3.86 GPa to 5.75 GPa. Additionally, fully functionalized fibers exhibited the highest reduced modulus of 49.99 GPa, which is 274% of pristine fibers. Therefore, ZnO functionalization, besides being thermally helpful for the AM process, also affords persisting interfacial strength to the composite.

As seen through this study, the viscosity of the matrix must be kept within a range of fluidity. Silica nanoparticles distributed throughout the matrix aid greatly in the printing of epoxies. However, one problem with silica nanoparticles is that as the viscosity increases, the matrix material that forms the interface between the fibers and the rest of the matrix is hindered in its attempt to attach to the fibers, and the fibers are pre-impregnated in advance. In this way, the outer shell of the printing filament can be efficiently secured to the print bed while the interior of the filament is filled with lower viscosity materials that bond well to the carbon fibers.

The results from the samples created by this nozzle indicate that it is working as intended. To analyze the effectiveness of the nozzle, three 80 mN indents identical to the indentation function of the previous tests were made (Fig. 7g). The fiber was indented, followed by an indent made on the epoxy near the center of the nozzle cross-section. This was followed by an indent near the edge of the sample, where the silica particles are. The inner epoxy indentation load-depth plot peaks at the rightmost of the plot as it is the least stiff, but the stiffness of the epoxy on the outside is improved. The fiber held by the inner epoxy is well bonded (Fig. 7h). This technique can be expanded in future work to allow more types of materials to be printed extremely easily compared to traditional methods. The simple design of the nozzle ensures that extra complexity is kept to a minimum so that the rapid pace of this method of composite manufacturing can stay unchanged.

4. Conclusions

This study utilized a coaxial nozzle combined with a fiber surface modification technique to enhance the direct ink writing capabilities in the manufacturing of continuous fiber-reinforced thermosetting polymer composites. Our significant contributions were that we proposed the concept of how fiber surface modification aids in the 3D printing of composite materials and realized an expanded printable range of thermosetting materials. By investigating the improved thermal conductivity of functional fibers, we enhanced the 3D printing capabilities of thermosetting composites. Furthermore, through rheological control and process parameter optimization, we achieved in-situ curing, enhancing printing accuracy. Testing on the interfacial behavior between ZnO functionalized fibers and matrix materials also indicated that the hydrothermal chemical growth of ZnO nanowires is an effective method to enhance the interfacial mechanical properties of carbon fiber composites. These advancements support applications such as electromagnetic interference shielding, piezoelectric energy harvesting, energy storage devices, advanced sensor technologies, and structural components in aerospace industries.

CRediT authorship contribution statement

Zhuoyuan Yang: Writing review & editing, Writing original draft, Methodology, Investigation, Formal analysis, Conceptualization. **Evan Medora:** Writing original draft, Methodology, Investigation, Conceptualization. **Zefu Ren:** Investigation, Methodology. **Meng Cheng:** Writing review & editing, Formal analysis. **Sirish Namilae:** Writing review & editing, Project administration, Methodology, Formal analysis, Conceptualization. **Yizhou Jiang:** Writing review & editing, Project administration, Methodology, Formal analysis, Conceptualization.

Declaration of competing interest

The authors declare that they have no known competing financial interests or personal relationships that could have appeared to influence the work reported in this paper.

Data availability

Data will be made available on request.

Acknowledgments

We acknowledge Dr. Daewon Kim for the help with optical imaging. We acknowledge Mr. Yuxuan Wu for SEM imaging. We acknowledge Mr. Hang Song for assisting in CAD design. Meng Cheng acknowledges the funding support through the National Natural Science Foundation of China under grant no. 52201272 and the Hubei Provincial Natural Science Foundation of China under grant no. 2022CFB625. Sirish Namilae acknowledges the funding support through the National Science Foundation under grant no. 2018375 and 2001038. Yizhou Jiang acknowledges the ERAU Faculty Innovative Research in Science and Technology Program and ERAU COE-Boeing CAAS Seed Grant.

Appendix A. Supplementary data

Supplementary data to this article can be found online at https://doi.org/10.1016/j.compscitech.2024.110782.

References

[1] D.K. Rajak, D.D. Pagar, P.L. Menezes, E. Linul, Fiber-reinforced polymer composites: manufacturing, properties, and applications, Polymers 11 (10) (2019) 1667.
[2] P. S, S. Km, N. K, S. S, Fiber reinforced composites - a review, J. Mater. Sci. Eng. 6 (2017) 1 6.
[3] M. Liu, Y. Chen, W. Cheng, S. Chen, T. Yu, W. Yang, Controllable electromechanical stability of a torsional micromirror actuator with piezoelectric composite structure under capillary force, Capillarity 5 (3) (2022) 51 64.
[4] X. Ding, H. Kong, M. Qiao, L. Zhang, M. Yu, Surface modification of an aramid fiber via grafting epichlorohydrin assisted by supercritical CO2, RSC Adv. 9 (53) (2019) 31062 31069.

[5] A.B. Strong, Fundamentals of Composites Manufacturing: Materials, Methods and Applications, Society of Manufacturing Engineers, 2008.
[6] P.K. Mallick, Fiber-reinforced Composites: Materials, Manufacturing, and Design, CRC press, 2007.
[7] C. Liu, W. Wu, D. Drummer, W. Shen, Y. Wang, K. Schneider, F. Tomiak, ZnO nanowire-decorated Al2O3 hybrids for improving the thermal conductivity of polymer composites, J. Mater. Chem. C 8 (16) (2020) 5380 5388.
[8] X. Chen, S. Cheng, K. Wen, C. Wang, J. Zhang, H. Zhang, H. Ma, L. Wu, T. Li, B. Li, J. Shao, In-situ damage self-monitoring of fiber-reinforced composite by integrating self-powered ZnO nanowires decorated carbon fabric, Compos. B Eng. 248 (2023) 110368.
[9] T.D. Ngo, A. Kashani, G. Imbalzano, K.T.Q. Nguyen, D. Hui, Additive manufacturing (3D printing): a review of materials, methods, applications and challenges, Compos. B Eng. 143 (2018) 172 196.
[10] M. Gebler, A.J.M. Schoot Uiterkamp, C. Visser, A global sustainability perspective on 3D printing technologies, Energy Pol. 74 (2014) 158 167.
[11] P. Parandoush, D. Lin, A review on additive manufacturing of polymer-fiber composites, Compos. Struct. 182 (2017) 36 53.
[12] Y. Chen, Z. Jin, W. Kang, Z. Liu, W. Yang, Y. Li, 3D printed bio-inspired self-similar carbon fiber reinforced composite sandwich structures for energy absorption, Compos. Sci. Technol. 248 (2024) 110453.
[13] J. Zhao, Q. Li, F. Jin, N. He, Digital light processing 3D printing Kevlar composites based on dual curing resin, Addit. Manuf. 41 (2021) 101962.
[14] R. Xiao, M. Ding, Y. Wang, L. Gao, R. Fan, Y. Lu, Stereolithography (SLA) 3D printing of carbon fiber-graphene oxide (CF-GO) reinforced polymer lattices, Nanotechnology 32 (23) (2021) 235702.
[15] R. Matsuzaki, M. Ueda, M. Namiki, T.-K. Jeong, H. Asahara, K. Horiguchi, T. Nakamura, A. Todoroki, Y. Hirano, Three-dimensional printing of continuous-fiber composites by in-nozzle impregnation, Sci. Rep. 6 (1) (2016) 23058.
[16] J. Zhang, W. Yang, Y. Li, Process-dependent multiscale modeling for 3D printing of continuous fiber-reinforced composites, Addit. Manuf. 73 (2023) 103680.
[17] P.J. Hine, H. Rudolf Lusti, A.A. Gusev, Numerical simulation of the effects of volume fraction, aspect ratio and fibre length distribution on the elastic and thermoelastic properties of short fibre composites, Compos. Sci. Technol. 62 (10) (2002) 1445 1453.
[18] J. Liu, Z. Yue, H. Fong, Continuous nanoscale carbon fibers with superior mechanical strength, Small 5 (5) (2009) 536 542.
[19] D.D.L. Chung, Processing-structure-property relationships of continuous carbon fiber polymer-matrix composites, Mater. Sci. Eng. R Rep. 113 (2017) 1 29.
[20] A. Thakur, X. Dong, Printing with 3D continuous carbon fiber multifunctional composites via UV-assisted coextrusion deposition, Manufact. Lett. 24 (2020) 1 5.
[21] M. Heidari-Rarani, M. Rafiee-Afarani, A.M. Zahedi, Mechanical characterization of FDM 3D printing of continuous carbon fiber reinforced PLA composites, Compos. B Eng. 175 (2019) 107147.
[22] E. Vivaldo-Lima, E. Saldívar-Guerra, Handbook of Polymer Synthesis, Characterization, and Processing, John Wiley & Sons, 2013. Incorporated.
[23] Y. Sun, L. Wang, Y. Ni, H. Zhang, X. Cui, J. Li, Y. Zhu, J. Liu, S. Zhang, Y. Chen, M. Li, 3D printing of thermosets with diverse rheological and functional applicabilities, Nat. Commun. 14 (1) (2023) 245.
[24] B.G. Compton, J.A. Lewis, 3D-Printing of lightweight cellular composites, Adv. Mater. 26 (34) (2014) 5930 5935.
[25] X. He, Y. Ding, Z. Lei, S. Welch, W. Zhang, M. Dunn, K. Yu, 3D printing of continuous fiber-reinforced thermosetting composites, Addit. Manuf. 40 (2021) 101921.
[26] T.-T.-L. Doan, H. Brodowsky, E. Mäder, Jute fibre/epoxy composites: surface properties and interfacial adhesion, Compos. Sci. Technol. 72 (10) (2012) 1160 1166.
[27] R. Kumar, R. Singh, M. Singh, P. Kumar, ZnO nanoparticle-grafted PLA thermoplastic composites for 3D printing applications: tuning of thermal, mechanical, morphological and shape memory effect, J. Thermoplast. Compos. Mater. 35 (6) (2020) 799 825.
[28] N. Vidakis, M. Petousis, A. Maniadi, E. Koudoumas, G. Kenanakis, C. Romanitan, O. Tutunaru, M. Suchea, J. Kechagias, The mechanical and physical properties of 3D-printed materials composed of ABS-ZnO nanocomposites and ABS-ZnO microcomposites, Micromachines 11 (6) (2020) 615.
[29] S. Tiwari, J. Bijwe, Surface treatment of carbon fibers - a review, Procedia Tech. 14 (2014) 505 512.
[30] Y. Lin, G. Ehlert, H.A. Sodano, Increased interface strength in carbon fiber composites through a ZnO nanowire interphase, Adv. Funct. Mater. 19 (16) (2009) 2654 2660.
[31] S. Madhu, A.J. Anthuuvan, S. Ramasamy, P. Manickam, S. Bhansali, P. Nagamony, V. Chinnuswamy, ZnO nanorod integrated flexible carbon fibers for sweat cortisol detection, ACS Appl. Electron. Mater. 2 (2) (2020) 499 509.
[32] H. Zhu, K. Fu, T. Huang, H. Liu, B. Yang, Y. Zhou, Y. Li, Highly conductive CFRP composite with Ag-coated T-ZnO interlayers for excellent lightning strike protection, EMI shielding and interlayer toughness, Compos. B Eng. 279 (2024) 111448.
[33] U. Galan, Y. Lin, G.J. Ehlert, H.A. Sodano, Effect of ZnO nanowire morphology on the interfacial strength of nanowire coated carbon fibers, Compos. Sci. Technol. 71 (7) (2011) 946 954.
[34] B. Wang, N. Li, S. Cheng, F. Hu, Q. Bao, H. Hao, C. Liu, Y. Chen, X. Jian, Enhance the thermal conductivity and mechanical properties of CF/PPBESK thermoplastic composites by growth ZnO nanowires with tunable length and diameter on prepreg, Polymer 244 (2022) 124662.
[35] X. Wu, J. Lee, V. Varshney, J.L. Wohlwend, A.K. Roy, T. Luo, Thermal conductivity of wurtzite zinc-oxide from first-principles lattice dynamics a comparative study with gallium nitride, Sci. Rep. 6 (1) (2016) 22504.
[36] D. Kumar, M.C. Dusabimana, M. Al-Haik, S. Namilae, Effect of nanoscale interface modification on residual stress evolution during composite processing, J. Compos. Mater. 57 (19) (2023) 2995 3011.
[37] A. Alipour Skandani, N. Masghouni, S.W. Case, D.J. Leo, M. Al-Haik, Enhanced vibration damping of carbon fibers-ZnO nanorods hybrid composites, Appl. Phys. Lett. 101 (7) (2012).
[38] F. Xie, W. Hu, D. Ning, L. Zhuo, J. Deng, Z. Lu, ZnO nanowires decoration on carbon fiber via hydrothermal synthesis for paper-based friction materials with improved friction and wear properties, Ceram. Int. 44 (4) (2018) 4204 4210.
[39] R.S. Rai, V. Bajpai, Hydrothermally grown ZnO NSs on Bi-Directional woven carbon fiber and effect of synthesis parameters on morphology, Ceram. Int. 47 (6) (2021) 8208 8217.
[40] N. Zheng, Y. Huang, W. Sun, X. Du, H.-Y. Liu, S. Moody, J. Gao, Y.-W. Mai, In-situ pull-off of ZnO nanowire from carbon fiber and improvement of interlaminar toughness of hierarchical ZnO nanowire/carbon fiber hydrid composite laminates, Carbon 110 (2016) 69 78.
[41] W. Lin, C. Yu, C. Sun, B. Wang, M. Niu, M. Li, W. Xuan, Q. Wang, Enhancing the thermal conductivity of epoxy composites via constructing oriented ZnO nanowire-decorated carbon fibers networks, Materials 17 (3) (2024) 649.
[42] Y. Jiang, J. Plog, A.L. Yarin, Y. Pan, Direct ink writing of surface-modified flax elastomer composites, Compos. B Eng. 194 (2020) 108061.
[43] B. Román-Manso, R.D. Weeks, R.L. Truby, J.A. Lewis, Embedded 3D printing of architected ceramics via microwave-activated polymerization, Adv. Mater. 35 (15) (2023) 2209270.
[44] S. Li, H. Zhang, Y. Han, Z. Lu, K. Miao, Z. Wang, D. Li, Thermally assisted extrusion-based 3D printing of continuous carbon fiber-reinforced SiC composites, Compos. Pt. A-Appl. Sci. Manuf. 172 (2023) 107593.
[45] K. Kong, B.K. Deka, S.K. Kwak, A. Oh, H. Kim, Y.-B. Park, H.W. Park, Processing and mechanical characterization of ZnO/polyester woven carbon fiber composites with different ZnO concentrations, Compos. Pt. A-Appl. Sci. Manuf. 55 (2013) 152 160.
[46] X. Meng, J. Li, H. Cui, L. Ye, C. Zhang, Y. Li, Loading rate effect of the interfacial tensile failure behavior in carbon fiber epoxy composites toughened with ZnO nanowires, Compos. B Eng. 212 (2021) 108676.
[47] B.-J. Kim, S.-H. Cha, K. Kong, W. Ji, H.W. Park, Y.-B. Park, Synergistic interfacial reinforcement of carbon fiber/polyamide 6 composites using carbon-nanotube-modified silane coating on ZnO-nanorod-grown carbon fiber, Compos. Sci. Technol. 165 (2018) 362 372.
[48] T. Wu, X. Huan, X. Jia, G. Sui, L. Wu, Q. Cai, X. Yang, 3D printing nanocomposites with enhanced mechanical property and excellent electromagnetic wave absorption capability via the introduction of ZIF-derivative modified carbon fibers, Compos. B Eng. 233 (2022) 109658.
[49] S. Zhandarov, E. Mäder, Characterization of fiber/matrix interface strength: applicability of different tests, approaches and parameters, Compos. Sci. Technol. 65 (1) (2005) 149 160.
[50] Y. Zhou, M. Fan, L. Chen, Interface and bonding mechanisms of plant fibre composites: an overview, Compos. B Eng. 101 (2016) 31 45.
[51] A. Kelly, W.R. Tyson, Tensile properties of fibre-reinforced metals: copper/tungsten and copper/molybdenum, J. Mech. Phys. Solid. 13 (6) (1965) 329 350.
[52] L.S. Penn, E.R. Bowler, A new approach to surface energy characterization for adhesive performance prediction, Surf. Interface Anal. 3 (4) (1981) 161 164.
[53] D.B. Marshall, An indentation method for measuring matrix-fiber frictional stresses in ceramic composites, J. Am. Ceram. Soc. 67 (12) (1984). C-259-C-260.
[54] B. Rohrmüller, P. Gumbsch, J. Hohe, Calibrating a fiber matrix interface failure model to single fiber push-out tests and numerical simulations, Compos. Pt. A-Appl. Sci. Manuf. 150 (2021) 106607.
[55] M.S. Goodarzi, H. Hosseini-Toudeshky, H. Ghashochi-bargh, Nanoindentation characterization of Glass/Epoxy composite for viscoelastic damage interlaminar modeling, Eng. Fract. Mech. 226 (2020) 106873.
[56] Q. Li, Y. Li, L. Zhou, Nanoscale evaluation of multi-layer interfacial mechanical properties of sisal fiber reinforced composites by nanoindentation technique, Compos. Sci. Technol. 152 (2017) 211 221.
[57] Y. Li, M. Li, Y. Gu, Z. Zhang, P. Guan, Investigation of the nanoscale mechanical properties of carbon fiber/epoxy resin interphase. I. analysis of fiber-stiffening effect during the nanoindentation process based on numerical simulation, Polym. Compos. 33 (8) (2012) 1387 1394.
[58] Y. Sun, D. Zuo, L. Cao, W. Lu, Y. Zhu, J. Li, Characterization of Carbon Fiber Reinforced Resin Composites by the Nanoindentation Technique, 2013. SPIE.
[59] W.M. Mueller, J. Moosburger-Will, M.G.R. Sause, S. Horn, Microscopic analysis of single-fiber push-out tests on ceramic matrix composites performed with Berkovich and flat-end indenter and evaluation of interfacial fracture toughness, J. Eur. Ceram. Soc. 33 (2) (2013) 441 451.
[60] S.-H. Lee, S. Wang, G.M. Pharr, H. Xu, Evaluation of interphase properties in a cellulose fiber-reinforced polypropylene composite by nanoindentation and finite element analysis, Compos. Pt. A-Appl. Sci. Manuf. 38 (6) (2007) 1517 1524.